Liquid Crystals
Publication details, including instructions for authors and subscription information:
http://www.informaworld.com/smpp/title~content=t713926090

Synthesis, characterisation and behaviour under a field of a chiral smectic liquid crystal

T. Soltani[a]; N. Bitri[a]; H. Dhaouadi[a]; A. Gharbi[a]; J. P. Marcerou[b]; H. T. Nguyen[b]
[a] Laboratoire de Physique de la Matière Molle Faculté des Sciences de Tunis 2092 El Manar TUNIS, Tunisie [b] Centre de Recherches Paul Pascal, Pessac, France

First published on: 08 October 2009

To cite this Article Soltani, T. , Bitri, N. , Dhaouadi, H. , Gharbi, A. , Marcerou, J. P. and Nguyen, H. T.(2009) 'Synthesis, characterisation and behaviour under a field of a chiral smectic liquid crystal', Liquid Crystals, 36: 12, 1329 — 1336, First published on: 08 October 2009 (iFirst)
To link to this Article: DOI: 10.1080/02678290903220998
URL: http://dx.doi.org/10.1080/02678290903220998

Liquid Crystals,
Vol. 36, No. 12, December 2009, 1329–1336

Taylor & Francis
Taylor & Francis Group

Synthesis, characterisation and behaviour under a field of a chiral smectic liquid crystal

T. Soltani[a]*, N. Bitri[a], H. Dhaouadi[a], A. Gharbi[a], J.P. Marcerou[b] and H.T. Nguyen[b]

[a]*Laboratoire de Physique de la Matière Molle Faculté des Sciences de Tunis 2092 El Manar TUNIS, Tunisie;* [b]*Centre de Recherches Paul Pascal, 115 Avenue Albert-Schweitzer, 33600 Pessac, France*

(Received 6 June 2009; final form 30 July 2009)

The C12HH compound has been synthesised and the phase transition temperatures were obtained by combining several experimental techniques. This compound exhibits in volume all of the tilted smectic phases except the SmC^*_α phase and presents a large SmC* range. The experimental results show unexpected behaviour in planar cell capacitors: (i) compared with the bulk, the SmC* range extends to lower temperature where it coexists with another phase; this demixing phenomenon is not due to a thickness effect but probably induced by a polarisation effect; (ii) the unwinding process of the ferroelectric SmC* phase occurs via two steps with an intermediate state (or phase). The $E-T$ diagram of C12HH has been established except in the region where the coexistence occurs.

keywords: liquid crystal; ferroelectric; coexistence; phase diagram

1. Introduction

The remarkable behaviour of ferroelectric liquid crystals is not only fundamentally interesting but also very attractive from an application point of view. This is due to the diverse phases that can appear when the temperature changes. The most general phase sequence when lowering the temperature is $SMA-SmC^*_\alpha - SMC^*-SmC^*_{Fi2} - SmC^*_{Fi1} - SmC^*_A$. In the ferroelectric SmC* phase the molecules are tilted at an angle θ from the layer normal and the development of a spontaneous helical structure due to the chirality of the molecules leads the director to precess around the tilt cone. The direction of spontaneous electric polarisation $\vec{P}_S$ is perpendicular to both the layer normal $\vec{z}$ and the director $\vec{n}$ while the magnitude is to first-order proportional to θ. For the rest of the phases the distribution of the azimuthal direction is periodic with a unit cell of two layers in SmC^*_A, three in SmC^*_{Fi1}, four in SmC^*_{Fi2} or more in SmC^*_α (see (*1,2*)). In most of these phases the layer normal is a symmetry axis so there is no macroscopic polarisation except for the SmC^*_{Fi1} phase in which the average of the long axis is tilted. All of the tilted phases have a helical structure and the sense of the helix is opposite in the SmC* and the SmC^*_A phases.

The structures of the subphases are almost completely known, but many complex phenomena are still not understood. So the experimental and theoretical studies are still interesting. The study and characterisation of these phases including chemical aspects seem to be necessary. The main difficulty met by the physicist is the availability of liquid crystal compounds. In our laboratory we have decided to synthesise a ferroelectric liquid crystal having the molecular structure shown in Figure 1. The synthesis of the (S)-1-methylheptyl-4[4-(4-dodecyloxybenzoyloxy)-benzoyloxy] benzoate (C12HH) was described in detail in (*3*). The C12HH has been chosen for two reasons: first because it exhibits a very rich polymorphism with the formation of SmA, SmC*, SmC^*_{Fi2}, SmC^*_{Fi1} and SmC^*_A phases; and, second, because of its large ferroelectric SmC* range.

2. Characterisation

The phase transition temperatures in bulk samples were obtained by the optical microscopic observation, differential scanning calorimetry (DSC), transmitted light and the optical rotatory power (ORP) measurements. Slight differences between these methods are in part due to instrument factors and difficulties in distinguishing some transitions.

2.1 DSC

DSC was performed in the cooling and heating runs at scanning rates of 1–3°C min^{-1}. Figure 2 shows a typical thermogram for C12HH. Three peaks were observed indicating the existence of the SmC*, SmC^*_{Fi} and SmC^*_A phases.

2.2 Microscopic observation

In the microscopic observation and the DSC cooling and heating scans all intermediate phases were detected but the SmC^*_{Fi1} and SmC^*_{Fi2} could not be distinguished from each other (Figure 2). On cooling from the isotropic liquid the homeotropic and focal

*Corresponding author. Email: tawfik_sol@yahoo.fr

ISSN 0267-8292 print/ISSN 1366-5855 online

DOI: 10.1080/02678290903220998
http://www.informaworld.com

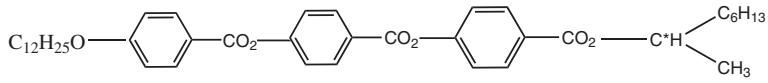

Figure 1. The molecular structure of C12HH.

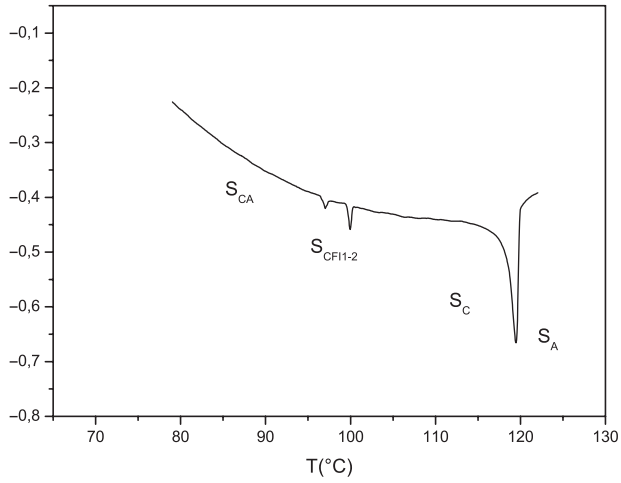

Figure 2. DSC diagram of C12HH at a cooling rate of 1°C min^{-1}.

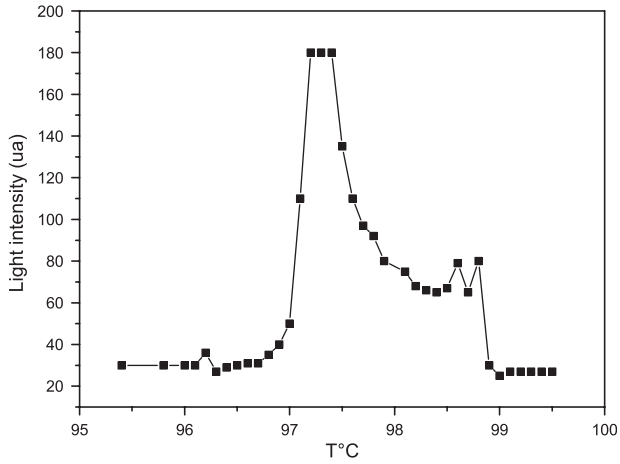

Figure 3. Temperature dependence of transmitted light at a cooling rate of 0.2°C min^{-1}.

conics textures of a SmA phase are found. Then the ferroelectric phase appears with a striated fan-shaped or coloured pseudo-homeotropic texture. Further cooling produces a typical ferrielectric texture in the homeotropic part of the cell. The texture constantly moves. As the temperature is decreased the anticlinic phase appears showing large stripes.

2.3 Transmitted light

Figure 3 shows the temperature dependence of transmitted light intensity in a homeotropic sample, we observe the transition SmC*–SmC^*_{Fi2} at 100°C, while the SmC^*_A phase is stable below 96.5°C. In contrast to DSC the SmC^*_{Fi1}–SmC^*_{Fi2} transition was clearly observed at about 97.5°C.

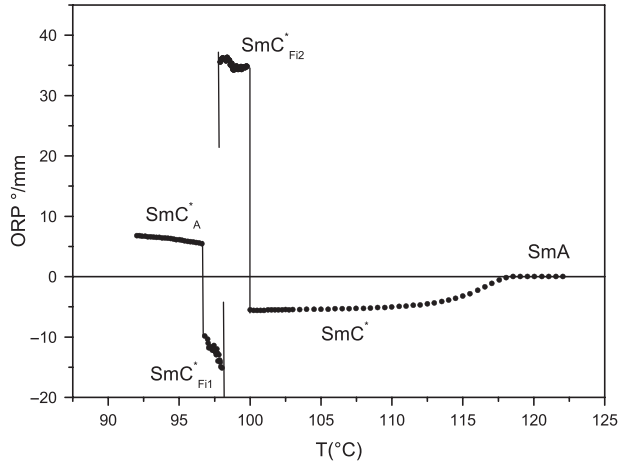

Figure 4. Optical rotatory power for $d = 100\mu m$ thick sample of C12HH.

2.4 Optical rotatory power and birefringence

The ORP and birefringence of this compound were measured with the 632.8 nm He–Ne laser source for a thick (100 μm) sample aligned in the homeotropic geometry between two glass plates which have been treated with a polymer. In figures 4 and 5 we respectively present the experimental results of the ORP and birefringence. All the measurements were carried out at stabilised temperatures. The ORP and birefringence behaviour change at the same temperature (≈ 119°C). This indicates the direct transition between SmA and SmC* phases without SmC^*_α because in this latter phase the birefringence should decrease while exhibiting no ORP (*4*). The SmC* phase (100–119°C) shows a negative ORP which changes its sign at the $SmC^* - SmC^*_{Fi2}$ phase transition due to the increase of the pitch. We can distinguish between the SmC^*_{Fi2} and SmC^*_{Fi1} phases by another sign change at 98°C, which indicates that the helical twisting changes its sense at this phase transition. Then a final sign change occurs at the SmC^*_A–SmC^*_{Fi1} phase transition due to the decrease of the pitch.

If we combine the different results from the experimental techniques we can conclude that the phase

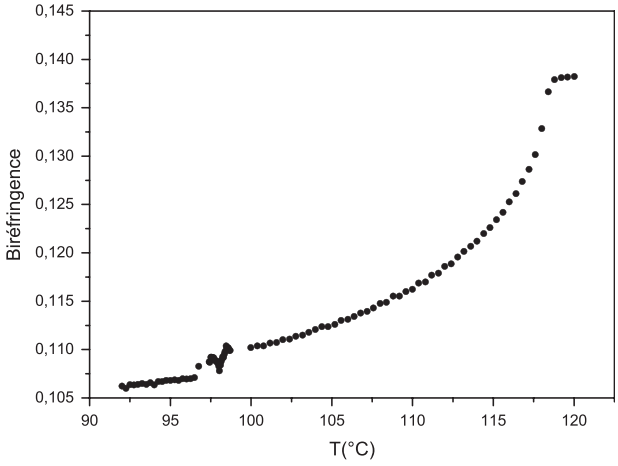

Figure 5. Birefringence for a 100μm thick sample of C12HH.

sequence and transition temperatures for the bulk sample are

I (131) SmA (119) SmC* (100) SmC^*_{Fi2} (98) SmC^*_{Fi1} (96.5) SmC^*_A which agree with the latest data found in the literature (*5*).

3. Phase diagram

The field-induced phase transitions for several compounds have been investigated extensively through dielectric measurement under a dc electric field (*6*), constant current (*6,7*), field-induced apparent angle (*8,9*), electro-optical (*6,7*) and optical transmittance (*10,11*). The studied compounds such as C10F3 and C7F2 exhibit a phase sequence without a polar SmC* phase. So the study of other compounds which present a sequence with this polar phase seems to be necessary in order to enrich the characterisation of the subphases in the presence of a dc electric field.

The first requirement to build the phase diagram (*E–T*) for the sample is the localisation of the successive phases without electric field. However, much attention must be paid to effects that can be misleading. In thin (2 μm) planar cells a coexistence of ferroelectric SmC* and anticlinic SmC^*_A phases was observed by Hatano *et al.* through an optical transmittance hysteresis loop in MHPOBC (*10*). They claimed that this phenomenon appears in the case of weak thickness but that for thick samples (more than 15 μm) it disappears and all of the bulk phases are detected (*10*).

The microscopic observation, dielectric measurements, electro-optic and constant current experiments have been performed using commercial cells (EHC, Japan) coated with indium tin oxide (ITO). The thicknesses of the cells were 3, 6 and 16 μm. The active area was 25 mm^2. The cells were filled with liquid crystals by a capillary action from the isotropic phase. A good planar alignment was obtained by slowly cooling the sample from isotropic to SmA phase.

The complex dielectric constant $\varepsilon^* = \varepsilon' - j\varepsilon''$ was measured with an impedance meter having the frequency range 10 Hz–200 kHz. A sinusoidal voltage modulation of 500 mVpp was applied. The Debye equation was used for fitting the experimental results in the following version (*12*):

$$\varepsilon'(\omega) = \varepsilon_\infty + \frac{\varepsilon_0 - \varepsilon_\infty}{1 + \omega^2\tau^2}, \quad (1)$$

$$\varepsilon''(\omega) = \frac{(\varepsilon_0 - \varepsilon_\infty)\omega\tau}{1 + \omega^2\tau^2}, \quad (2)$$

where ε' is the real part of the permittivity, ε'' its imaginary part, ω is the angular frequency of the applied field, and ε_0 and ε_∞ are the static and high-frequency dielectric permittivity, respectively.

3.1 *Phase sequence at zero field*

We first study the behaviour of our compound in a planar cell of 16 μm making a capacitor in order to ensure the presence and thickness dependence of the demixing phenomenon.

3.1.1 *Microscopic observations*

From our bulk characterisation we expect to see the disappearance of SmC* at 100°C but then it is still present below that temperature. Figure 6 illustrates the appearance of the SmC^*_A phase's texture with a green tint and its development within a few minutes at the temperature of 96.5°C. In fact there are two domains which correspond to a coexistence of two phases. To identify these phases we applied a sinusoidal electric field of frequency 2 Hz and amplitude 0.5 Vpp. The red area which is identified as the SmC* phase switches between two stable states ($+\theta$ for $E > 0$) or ($-\theta$ for $E < 0$) but no part in the green area changes. Figure 7 shows the texture change when the temperature decreases. On further cooling the proportion of anticlinic increases and the proportion of the ferroelectric (red area) decreases until it disappears at 92°C (Figure 7). The obvious interpretation is that the SmC* does not completely disappears at 100°C but coexists with another phase in the temperature range 92–100°C.

These observations have been made with a sample thickness of 16 μm, so, in contrast to the original reports (*10*), the demixing phenomenon is not characteristic of thin samples.

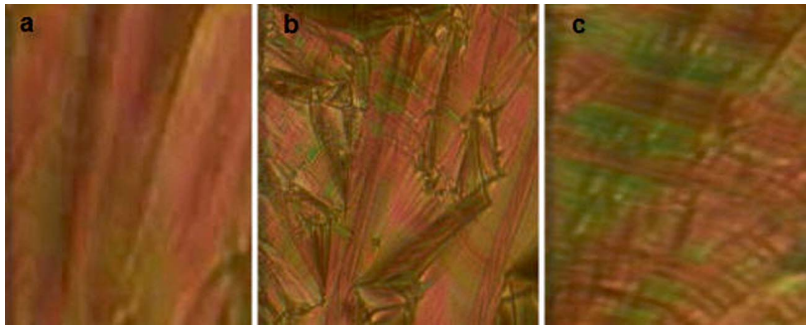

Figure 6. The time evolution of textures in the coexistence of phases at (a) $T = 96.5°C$, $t = 0$ s; (b) $T = 96.5°C$, $t = 12$ s; (c) $T = 96.5°C$, $t = 65$ s; thickness 16 μm.

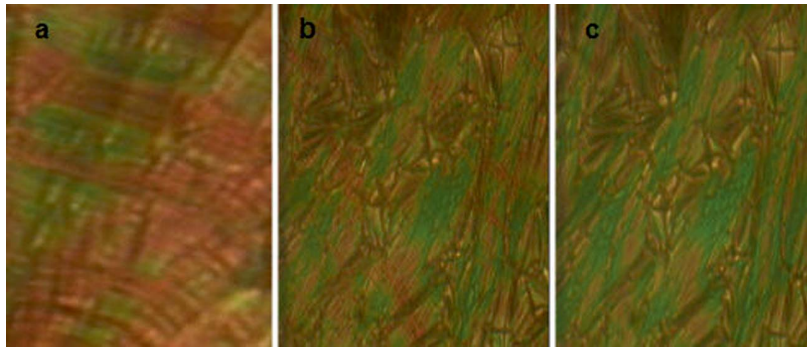

Figure 7. The final textures at (a) $T = 96.5°C$, (b) $T = 93°C$, (c) $T = 89°C$; thickness 16 μm.

3.1.2 *Dielectric study*

If one applies a small sinusoidal field without bias one can consider it to be only a small perturbation and use it to characterise the response at 'zero' field. We follow the behaviour of the Goldstone mode which is due to slight rotations of the macroscopic polarisation P_S on the SmC* cone and of the soft mode which is characteristic of the SmA to SmC* phase transition. The temperature dependence of the amplitude of Goldstone mode (A_G) and of the soft mode (A_S) extracted from the recorded relaxations in different phases is presented in Figure 8.

In the SmA phase the soft mode contribution to the dielectric response increases with decreasing temperature until the SmA–SmC* transition temperature is reached at 119°C. In the ferroelectric SmC* phase the Goldstone mode is characterised by the high value of its amplitude which remains constant. In the temperature range 92–100°C the amplitude of this mode gradually decreases with decreasing temperature and vanishes at 92°C (Figure 8 and 9). The relaxation process observed in this temperature range is a continuation of the Goldstone mode observed in the pure SmC* phase. Note that the Goldstone mode goes with the red colour observed in the temperature range 92–100°C and disappears when this colour vanishes

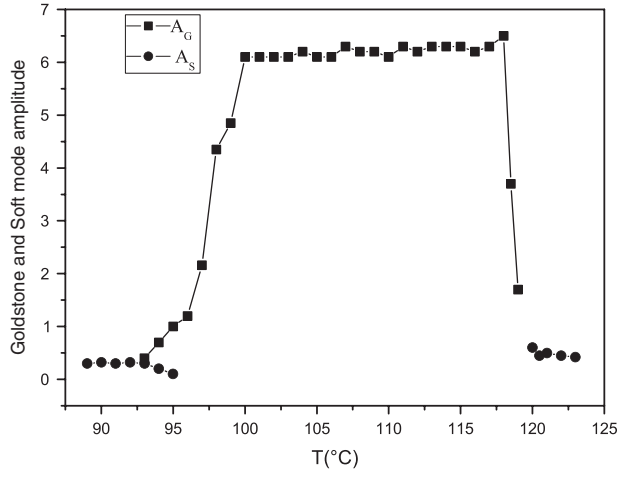

Figure 8. Temperature dependence of the amplitudes of Goldstone mode (A_G) and of the soft mode (A_S).

at 92°C. This confirms that the size of the Goldstone mode is in proportion with SmC* phase. We can conclude that the SmC* does not completely disappear at 100°C and in the temperature range ($96.5 \leq T \leq 100°C$) the sample is not in a pure ferrielectric phase like in the bulk, neither is it in the anticlinic phase for ($92 \leq T \leq 96.5°C$). There is

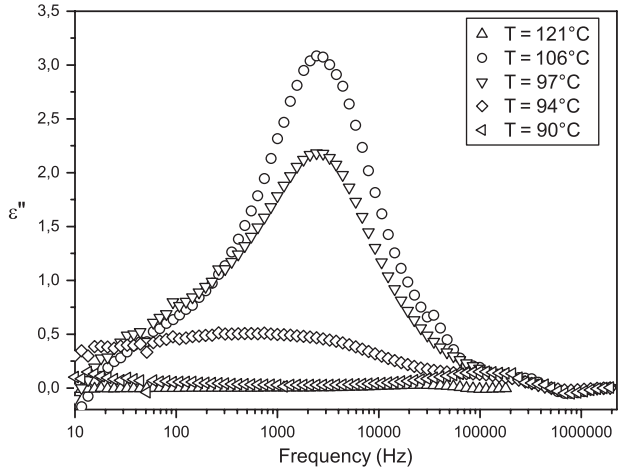

Figure 9. Frequency dependence of the imaginary part (ε'') of the dielectric constant for different temperatures.

instead a coexistence of the ferroelectric SmC* with another phase.

In order to confirm that this phenomenon is common in the liquid crystal family and to assert which of the ferroelectric SmC* phase or ferrielectric is responsible for its occurrence, two other compounds were investigated. The prototype liquid crystal MHPOBC exhibits the SmA–SmC^*_α–Sm*C**–SmC^*_{Fi1}–SmC^*_A phase sequence and the second compound, the (R) and (S)-12OF1M7, exhibits the same phase sequence as C12HH. The microscopic observation and the dielectric measurements show the same kind of coexistence between two phases. We also studied a mixture of MHPOBC (25% R; 75% S) which displays the SmA–Sm*C**–*Sm*C^*_A phase sequence. In this mixture a coexistence between ferroelectric and anticlinic phases has also been observed. We recall that the C10F3 (*6*) and C7F2 (*7*) which display a phase sequence without a ferroelectic phase are not subject to demixing phenomenon. So it is the ferroelectric SmC* phase and not the SmC^*_{Fi} which is responsible for of the demixing in planar samples.

In the present study a coexistence between ferroelectric and anticlinic phase was observed. In addition as expected, our experimental results show again the occurrence of this phenomenon in the thin planar cells (5 μm). This demixing phenomenon is not due to a thickness effect but it is probably induced by a polarisation effect as it is observed only when there is a ferroelectric SmC* phase in the bulk phase sequence.

To go further we have used the fact that our cell constitutes an electrical capacitor, observed under the microscope, that we could maintain in a state of an open or short circuit. We saw that each time there was a red SmC* domain, full size or in coexistence, the texture of the cell under open circuit conditions changed progressively but returned quickly to an original state when the circuit was shorted. We interpret this as due to the fact that the SmC* phase, which is initially in a wound state without bulk polarisation, on average develops in open circuit cells a partial polarisation by locally unwinding its helix. This polarisation is compensated for by charges at the electrodes in order to enforce the electrostatic equilibrium. As this phenomenon is also observed in the coexistence region we propose that in a planar capacitor the thermodynamical energy balance is more favourable with a mixing of the polarised SmC* with another phase than with the pure bulk phase. Moreover, we briefly compared the temperature domain of the coexistence in a part of the cell without ITO coating and found that it remains but is less extended (6.5°C instead of 8°C), showing that the demixing is dependent on the electrostatic conditions.

3.2 Transitions under an applied electric field

We now report on the part of the *E–T* phase diagram under a static field that we will show to be free of demixing phenomena as the presence of the electric field favours the monophasic domains.

3.2.1 Electro-optic studies

The electro-optical response for a field-induced phase transition was recorded for different temperatures. From this we can obtain the threshold fields when applying a rectangular wave of 50 Hz. It is defined as being the field from which the peak of polarisation appears or changes its amplitude suddenly. Figure 10 shows the field dependence of the macroscopic polarisation in the pure anticlinic and pure ferroelectric phases.

Above the monophasic domain of anticlinic SmC^*_A phase (Figure 10(a)), for a bias field E V μm^{-1}, the spontaneous polarisation is zero indicating that the anticlinic SmC^*_A phase is stable. Further field increases induce two abrupt changes of the polarisation which indicate that the two field-induced SmC^*_A–ferri and ferri–SmC* phase transitions take place, as already reported (*7,10*). In addition, when the dc field increases, the colour of the sample changes from green SmC^*_A to light green (ferri) then finally to the grey unwound SmC*.

Above the monophasic domain of the ferroelectric SmC* phase two distinct behaviours were observed. At high temperatures below SmA (114–119°C) only one jump was detected which indicates a direct transition to unwound SmC*. In addition this transition is detected by the microscopic observation of texture change, where two colours were observed when the

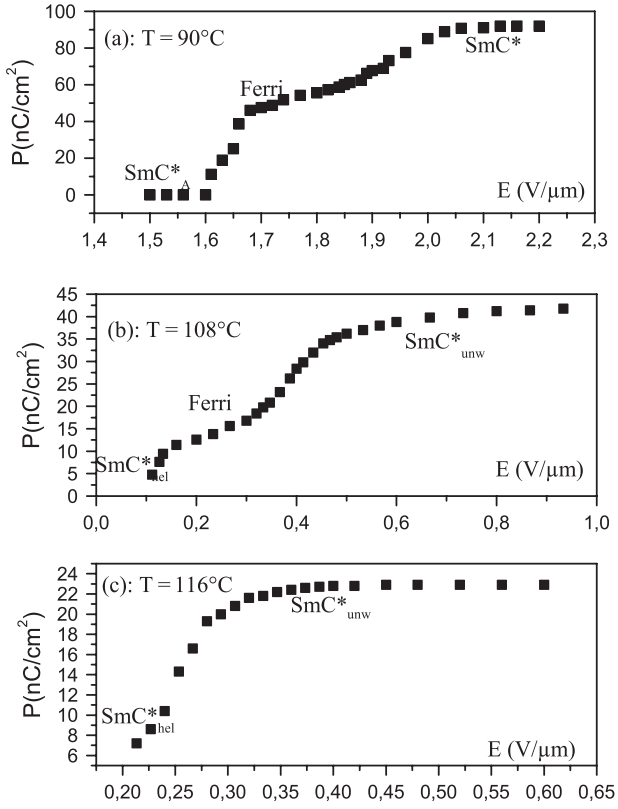

Figure 10. Field dependence of the polarisation for different temperatures.

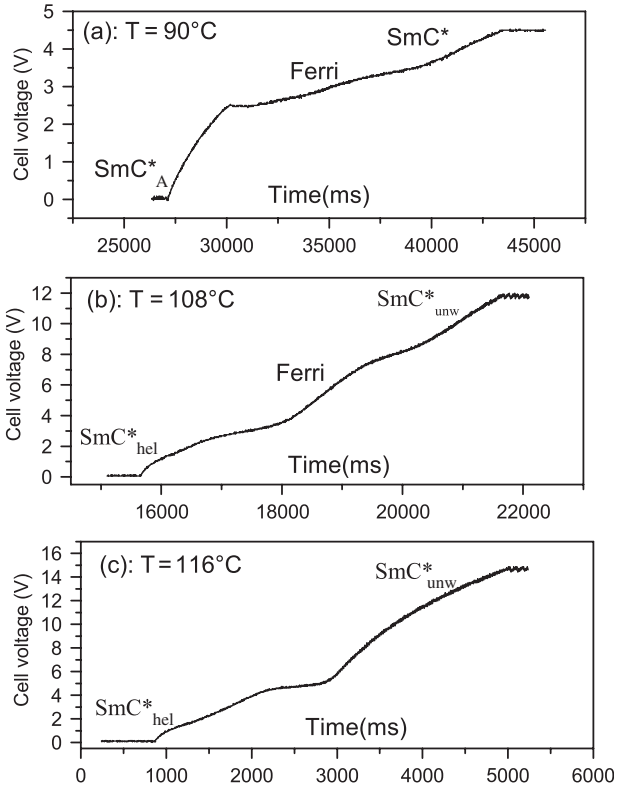

Figure 11. Typical curves showing the evolution of the cell voltage with time under a constant current of 4 nA.

electric field is increased. In the low-temperature range (100–114°C) two distinct jumps were detected. Over time three colours were observed when the electric field increased, from red to light green then finally to the grey SmC* tint.

3.2.2 *Constant current method*

The sample is connected to a Keithley current source delivering a constant current in the nanoampere range. The local field in the cells was recorded by the method presented by Marcerou *et al.* and given by the equation (*6*)

$$E = \frac{V}{e} = \frac{it}{\varepsilon_{\perp} S}, \tag{3}$$

where e is the cell thickness, S is the active surface, i is the current, $\varepsilon_{\perp}$ is the in-plane dielectric constant and t is the time.

The local field increases linearly with increasing time in a given phase. When there is a first-order transition, a plateau with a constant local field E_c appears with a duration Δt, except for the last plateau which reflects only the upper voltage limit set for the generator.

Figure 11 shows the time dependence of the field at a constant current of 4 nA.

Above the pure anticlinic SmC^*_A phase (below 92°C) we observed two plateaux which correspond to the phase transitions SmC^*_A–ferri and ferri–SmC* respectively (Figure 11(a)). Furthermore, the texture change is observed at the level of every phase transition.

Figures 11(b) and (c) show the result for the time dependence of local field in the SmC*. Two types of time dependence were observed: at higher temperature, near the SmA–SmC* phase transition (114–119°C), a single plateau is seen, showing the direct transition from the helical SmC* to the unwound SmC* phase (Figure 11(c)); at the lower temperature (100–114°C) two successive plateaux were found (Figure 11(b)) which is the same behaviour observed by the microscopic observation and by the electro-optic measurement. In order to understand the last case, two possibilities could be considered.

(1) The first plateau may be due to just a partial unwinding (reorientation) in SmC* which is not a phase transition, whereas the second plateau represents a transition to a completely unwound SmC* phase.
(2) The transition from the helical SmC* to the unwound SmC* phase would occur via an

intermediate phase. Therefore, this phase should be the ferrielectric phase SmC^*_{Fi1} as it presents the same light green tint as the SmC^*_{Fi1} phase in between SmC^*_A and SmC* phases.

As the three technique (electro-optic properties (Figure 10(c)), constant current method (Figure 10(b), and microscopic observation of texture change) show the same behaviour, we favour the second possibility and think that the two SmC* states, wound and unwound, are separated by a transient SmC^*_{Fi1} phase.

3.3 Complete phase diagram

The *E–T* phase diagram shown in Figure 12 has been established by combining electro-optic properties, microscopic observation, dielectric measurement and constant current method. Below $92°C$ where the pure anticlinic phase is stable, the field-induced phase sequence recorded by the different techniques is SmC*–ferri–SmC*. The temperature region between 92°C and 100°C corresponds to the demixing state. Then above the SmC* range, one observes the two successive regimes for helix unwinding. Near the SmA–SmC* phase transition temperature ($T \geq 119°C$) the SmA phase under the application of the static field becomes tilted (due to the electroclinic effect or soft mode (*12*)) and becomes the phase called SmC^*_{el} (see (*13*)). The first-order SmA–SmC* under an electric field and SmC^*_{el}–SmC^*_{unw} phase transitions were reported in (*13–16*).

4. Discussion

Our results confirm the existence of the demixing phenomenon in the liquid crystal exhibiting a ferroelectric phase, but we have shown that it does not disappear when increasing the sample thickness. This unexpected phenomenon is explained as follows: the ferroelectric phase is responsible for its occurrence and it is due to a polarisation effect and not to a thickness effect.

The two domains limited by the lines L_1 and L_2 and L_3 and L_1 in Figure 12 presenting the same light green color correspond to a ferrielectric phase: the first corresponds to the induced ferrielectric between anticlinic and unwound SmC* was also observed in the C7F2 by Essid *et al.* (*7*) and the sequence is in good agreement with the theoretical model reported by Dhaouadi (*17*). The second occurrence of a ferrielectric above the bulk SmC* is unexpected but it is confirmed by the different techniques. We point out that the same behaviour was observed also in the MHPOBC and in the (R)-12OBP1M.

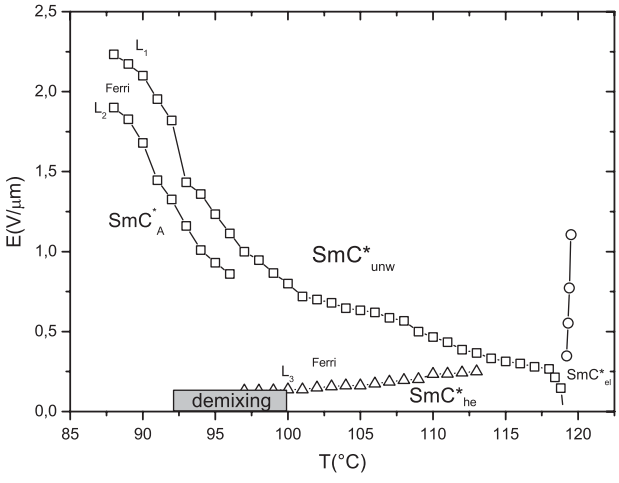

Figure 12. Final phase diagram for C12HH where the different experimental results are put together.

5. Conclusion

We have synthesised the C12HH compound and established the phase transition temperatures in the bulk by DSC, optical microscopy and ORP. Dielectric measurement and microscopic observation show clearly that the ferroelectric phase coexists in planar cells with another phase in the region where bulk ferrielectrics usually appear and with anticlinic SmC^*_A phase at around 4.5° C below the $SmC^*_{Fi1} - SmC^*_A$ phase transition point in the bulk. Moreover, the unusual experimental result found in the lower temperature range of SmC* phase remains to be understood.

Acknowledgements

We wish to acknowledge the support of CMCU grant # 06/G 1311 and CNRS/DGRSRT grant # 18476. We thank Marie France Achard. We are also grateful to Anne Hochedez and Stéphane Gineste for synthesising the samples (R) and (S)12OF1M7.

References

(1) Mach, P.; Pindak, R.; Levelut, A.M.; Barois, P.; Nguyen, H.T.; Huang, C.C.; Furenlid, L. *Phys. Rev. Lett.* **1998**, *81*, 1015–1018.
(2) Hirst, L.S.; Watson, S.J.; Gleeson, H.F.; Cluzeau, P.; Barois, P.; Pindak, R.; Pitney, J.; Cady, A.; Johnson, P.M.; Huang, C.C.; Levelut, A.M.; Srajer, G.; Pollmann, J.; Caliebe, W.; Seed, A.; Herbert, M.R.; Goodby, J.W.; Hird, M. *Phys. Rev. E* **2003**, *65*, 041705(1)–041705(10).
(3) Faye, V.; Rouillon, J.C.; Destrade, C.; Nguyen, H.T. *Liq. Cryst.* **1995**, *19*, 47–56.
(4) Bitri, N.; Gharbi, A.; Marcerou, J.P. *Physica B* **2008**, *403*, 3921–3928.

(5) Bibonne, F.; Parneix, J.; Nguyen, H.T. *Eur. Phys. J.* **1998**, *3*, 237–241.
(6) Marcerou, J.P.; Nguyen, H.T.; Bitri, N.; Gharbi, A.; Essid, S.; Soltani, T. *Eur. Phys. J. E* **2007**, *23*, 319–328.
(7) Essid, S.; Bitri, N.; Dhaouadi, H.; Gharbi, A.; Marcerou, J.P. *Liq. Cryst.* **2009**, *36*, 359–364.
(8) Bourny, V.; Orihara, H. *Phys. Rev. E* **2001**, *63*, 21703(1)–21703(7).
(9) Hiroki, K.; Takanishi, Y.; Skarp, K.; Takezoe, H.; Fukuda, A. *Jpn. J. App. Phy.* **1991**, *30*, 1819–1822.
(10) Hatano, J.; Harazaki, M.; Sato, M.; Iwauchi, K.; Saito, S.; Murashiro, K. *Jpn. J. App. Phys.* **1993**, *32*, 4344–4347.
(11) Orihara, H.; Naruse, Y.; Yagyu, M.; Fajar, A.; Uto, S. *Phys. Rev. E* **2005**, *72*, 040701(1)–040701(4).
(12) Garoff, S.; Meyer, R.B. *Phys. Rev. Lett.* **1977**, *38*, 848–851.
(13) Défontaines, A.; Prost, J. *Phys. Rev. E* **1993**, *47*, 1184–1198.
(14) Khened, S.M.; Prasad, S.K.; Shivkumar, B.; Sadashiva, B.K. *J. Phys. II* **1991**, *1*, 171–180.
(15) Dupont, L.; Galvan, J.; Marcerou, J.P.; Prost, J. *Ferroelectrics* **1988**, *84*, 317–325.
(16) Bahr, C.; Heppke, G. *Mol. Cryst. Liq. Cryst.* **1987**, *150b*, 313–324.
(17) Dhaouadi, H.; Bitri, N.; Essid, S.; Soltani, T.; Gharbi, A.; Marcerou, J.P. *Phys. Rev. E* **2009**, In press.